CONF-860605--30

DE87 000229

TENSILE AND FRACTURE PROPERTIES OF EBR-II-IRRADIATED V—15Cr—5Ti CONTAINING HELIUM*

M. L. Grossbeck and J. A. Horak

Metals and Ceramics Division, Oak Ridge National Laboratory
P.O. Box X, Oak Ridge, TN 37831 U.S.A.

ABSTRACT: The alloy V—15Cr—5Ti was cyclotron-implanted with 80 appm He and subsequently irradiated in the Experimental Breeder Reactor (EBR-II) to 30 dpa. The same alloy was also irradiated in the 10, 20, and 30% cold-worked conditions. Irradiation temperatures ranged from 400 to 700°C. No significant effects of helium on mechanical properties were found in this temperature range although the neutron irradiation shifted the temperature of transition from cleavage to ductile fracture to about 625°C. Ten percent cold work was found to have a beneficial effect in reducing the tendency for cleavage fracture following irradiation, but high levels (20%) were observed to reduce ductility. Still higher levels (30%) improved ductility by inducing recovery during the elevated-temperature irradiation. Swelling was found to be negligible, but precipitates — titanium oxides or carbonitrides — contained substantial cavities.

KEY WORDS: vanadium, helium, ductility, swelling, microstructure, fracture, tensile properties, embrittlement, irradiation

---

*Research sponsored by the Office of Fusion Energy, U.S. Department of Energy, under Contract No. DE-AC05-840R21400 with the Martin Marietta Energy Systems, Inc.

INTRODUCTION

Vanadium alloys have been studied for use as cladding and structural materials for fast reactors [1]. Although unalloyed vanadium is not particularly swelling resistant, many of its alloys, and particularly those containing titanium are very swelling resistant [2,3]. In addition to high swelling resistance, V—15Cr—5Ti has high creep strength. It is these properties combined with higher melting points than iron- and nickel-based alloys and compatibility with liquid alkali metals that make vanadium alloys, and in particular V—15Cr—5Ti, candidates for first wall and blanket structures in fusion reactors. This alloy and several others were investigated for fusion reactor application, but studies of these alloys waned because of high hydrogen diffusivity and solubility, resulting in high tritium inventory in the structures, and high tritium leakage. It is now believed that diffusion barriers can be employed to reduce leakage and that tritium can be removed from the first wall and blanket prior to its decommissioning. The disadvantage of tritium inventory is believed to be compensated for by the low neutron activation properties of vanadium alloys. Induced radioactivity is sufficiently low to allow direct trench burial upon decommissioning.

Fission reactors can be used to study the effects of radiation displacement damage on candidate fusion reactor materials, but the production of helium expected in a fusion reactor (~5 appm He/dpa) [4] must be simulated. Two methods that are employed to deposit helium in vanadium are the tritium trick [5], and accelerator implantation. Neither method is an ideal simulation of fusion reactor service, but

both methods complement each other and together provide required information on the effects of helium. In the tritium trick, tritium is diffused into the metal where it decays to ^{3}He. This method deposits helium at sites to which tritium diffuses and becomes trapped and is limited by the solubility and the decay constant of tritium. However, tritium will be present in vanadium structures in a fusion reactor so that at least some helium will result from just this mechanism. Accelerator implantation limits study to thin specimens and is a difficult and costly procedure, but deposition can be made homogeneous as is the case for helium produced by transmutations in a fusion reactor. Either method can be used to introduce helium, but neither method introduces helium simultaneously with neutron displacement damage. Such an experiment will not be possible until either a high flux 14 MeV neutron accelerator or an actual fusion device becomes available.

In the absence of such a device, the present experiment was designed to evaluate the effects of neutron irradiation and helium on the tensile and fracture properties of V—15Cr—5Ti. Helium was implanted with a cyclotron, then the specimens were irradiated in EBR-II. Post-irradiation tensile tests were then performed on the specimens. This type of experiment achieves both homogeneously distributed helium and atomic displacement damage thus simulating the two most important components of fusion reactor radiation.

A second part of this experiment evaluates the effect of cold work on V—15Cr—5Ti. When the effects of irradiation on the swelling and mechanical behavior of nonferrous alloys are evaluated, the nonferrous alloys in the annealed condition are most often compared with type 316

stainless steel in the 20% cold-worked condition. The cold-work study was done to provide data for a more relevant comparison of vanadium alloys with type 316 stainless steel. Additionally, the effects of cold work in irradiated V—15Cr—5Ti have not been previously investigated. In this phase of the experiment, 10, 20, and 30% cold-worked material was neutron irradiated, but no helium was implanted.

The postirradiation examination consisted of three phases. Tensile tests at the irradiation temperature were conducted to evaluate strength and ductility. These tests were followed by scanning electron microscopy to determine the mode of fracture. The third phase, transmission electron microscopy, was done to determine the reasons for the fracture behavior, in particular to determine the mechanism of the irradiation embrittlement.

EXPERIMENTAL PROCEDURE

Specimen material was prepared from a heat of V—15Cr—5Ti melted by Westinghouse Electric Corp. (heat HSV-307); the composition is given in Table I. Rolled sheet 0.25-mm thick was given a recrystallization anneal at 900°C for 0.5 h in a vacuum environment at a pressure of 0.5 to 2×10^{-7} torr ($0.7—3 \times 10^{-5}$ Pa). This heat treatment resulted in a grain size of 30 μm. The cold-worked material was prepared by annealing sheets at 900°C in thicknesses that resulted in 10, 20, and 30% reduction of area upon rolling to provide 0.25-mm-thick sheet.

The sheet was implanted with 52-MeV α-particles in the Oak Ridge Isochronous cyclotron. The sheet formed the front face of the irradiation chamber through which 18 to 20°C water flowed at a rate of

9.5×10^{-4} m^3/s. A rotating energy degrader was used to produce a uniform helium deposition over the entire thickness of the sheet. The beam was collimated to provide essentially uniform helium deposition over the region which was to become the gage sections of the specimens. In addition, the chamber was oscillated horizontally in front of the beam to irradiate the entire width of the sheet. Chemical analysis later indicated that a helium concentration of 80 appm was achieved.

A tensile specimen was designed to permit uniform α-particle deposition while still providing a valid measure of strength and ductility. The specimen design is shown in Fig. 1. The 0.25-mm thickness also made possible fabrication of tensile specimens by stamping with a precision die. The general reliability of the tensile specimen has been assessed and found satisfactory, although not as good as larger specimens, as reported by Klueh [6].

Following helium implantation the specimens were encapsulated in sodium and irradiated in subassembly X-287 in row 7 of EBR-II at 400, 525, 625, and 700°C. The capsules irradiated at the three highest temperatures contained zirconium foil as a getter. Each capsule was designed to operate isothermally, using a helium gas gap at 525°C and heat pipes at 625 and 700°C for temperature control. The 400°C capsules were in direct thermal contact with the reactor coolant. Differential thermal expansion monitors indicated that maximum temperatures of 425 and 525°C were attained in the 400 and 525°C capsules. The monitors in the 625 and 700°C capsules were damaged. A fluence of 4.8 to 5.5 $\times 10^{26}$ n/m^2 ($E > 0.1$ MeV) was obtained resulting in a damage level for

the specimens of 28 to 32 dpa. The helium level, 80 appm, corresponds to 16 dpa in a fusion reactor.

Following irradiation, the sodium was removed from the capsules using liquid anhydrous ammonia. Ammonia dissolves sodium without producing hydrogen and thus avoids the danger of introducing hydrogen into the specimens [7]. When the specimens appear free of sodium, they are washed with ethyl alcohol followed by water to remove residual sodium compounds.

All specimens were tested at the nominal irradiation temperatures on an Instron Model 1125 testing machine equipped with a vac-ion-pumped vacuum chamber. Pressures below 7×10^{-7} torr (9×10^{-5} Pa) were maintained during the test. The duration of exposure at elevated temperatures was minimized to prevent significant contamination by oxygen during the test. Preliminary tests were conducted to confirm that the vacuum was sufficient to prevent oxygen contamination during testing.

Scanning electron microscope (SEM) fractography was done on an Amray 1200B SEM extensively modified for remote operation in a radiation hot cell [8]. Transmission electron microscopy (TEM) was performed on a JEOL 100CX using an accelerating voltage of 120 kV.

Experimental Results

Tensile Properties

Results of the tensile tests appear in Table II. Strength levels for annealed material are plotted in Fig. 2 for four conditions: helium-injected, neutron-irradiated, helium-injected plus neutron-irradiated, and control material without either irradiation or implantation. Helium implantation does not significantly alter the strength.

However, neutron irradiation increases strength by about a factor of 2 at 400°C and about 50% at 700°C. The neutron-irradiated, helium-injected material has similar strength to the neutron-irradiated material.

Helium has a larger effect on ductility as shown by Fig. 3. Helium alone has an effect only at 400°C where it reduces ductility by about a factor of 2; elongations are approximately the same as unimplanted material at higher temperatures. Neutron irradiation reduces tensile elongations to below 1%, and neutron irradiation of helium-implanted material reduces elongation to about 2%. The difference is probably not significant.

The cold-worked material was neutron-irradiated, but none was helium-implanted. By comparison of Figs. 4 through 6, the effect of cold work on strengthening is observed to saturate by a cold-work level of 20%. Since the controls were not aged at the irradiation temperatures, the differences between the curves for irradiated material and the curves for the control material represent a combination of thermal exposure and irradiation. The curves show the effect of radiation strengthening at 400°C and, in some cases, at 525°C. In general, irradiation increased the yield and ultimate strengths for cold-worked material to about the same levels as those for annealed material. However, strength decreases rapidly with increasing temperature, and in the case of 30%-cold-worked material, the additional strain energy appears to have been sufficient to induce a degree of recovery resulting in strength levels characteristic of the annealed material. The effect of irradiation on ductility appears to be slight, with the exception

that uniform and total elongation become nearly equal, especially at the lower temperatures.

Ductility as measured by uniform and total elongation is reduced by about a factor of 4 by cold working and appears to saturate at a cold-work level of 10% or less (Fig. 7 through 9). What is more significant is that, following neutron irradiation, the cold-worked material is more ductile than the annealed material at all temperatures investigated. This is especially true at 700°C where total elongations for cold-worked material are about six times those of annealed material.

The effects of cold work can be seen better by plotting tensile properties as a function of cold-work level. Two properties, 0.2% yield strength and total elongation, have been selected and plotted as a function of degree of cold work. Figures 10 shows yield strength as a function of cold work for unirradiated V—15Cr—5Ti. The curves indicate the expected strengthening and slight recovery during testing at 525 and 700°C at the 30%-cold-work level. The yield strength of the irradiated material (Fig. 11) is also well behaved showing strengthening at 400°C and recovery during irradiation at 525 and 700°C. The recovery becomes more complete as the level of cold work increases.

Ductility of the unirradiated material corresponds to the yield strength in that stronger material is less ductile. Figure 12 illustrates a large reduction in ductility in going from annealed material to 10% cold-worked material. At 10% cold work, total elongation saturates then exhibits slight recovery at a cold-work level of 30%. Following irradiation, the alloy displays rather unusual behavior as shown in Fig. 13.

At 400°C ductility is nearly constant. At 525 and 700°C, adding 10%-cold work results in a very large increase in ductility. This ductility is reduced to that of the annealed material if the alloy is reduced 20% by rolling but returns if the alloy is further reduced by 30%-cold work. This phenomenon is not yet understood but will be discussed later.

Fracture Surface Morphology

The general fracture surface morphology is tabulated in Table III and correlates well with tensile ductility. All of the unirradiated specimens failed by ductile rupture, even if implanted with helium. The fracture surfaces of the neutron-irradiated specimens showed mechanisms ranging from ductile rupture (Fig. 14) to total cleavage in the case of specimens fractured in an uncontrolled fashion at room temperature (Fig. 15). Helium implantation, which was found to have little effect on strength and ductility, did not alter the mode of fracture although ductility appeared to be more limited than for unimplanted, unirradiated specimens. Neutron irradiation, however, resulted in cleavage fracture at 400°C in annealed material, quasi-cleavage at 625°C, and only at 700°C did ductile rupture become evident (Fig. 16). Note that in discussing this progression the helium-injected, neutron-irradiated material was treated the same as neutron-irradiated material since helium injection appeared to have no significant effect. The presence of cleavage fracture at the lowest temperature and complete disappearance at 700°C indicates a transition in fracture mechanism. The intermediate-type morphology, known as quasi-cleavage, at 625°C is evidence that the transition temperature is near this value.

The fracture morphology of the cold-worked material also reflected mechanical behavior, but the effects were not as apparent. In 10%-cold-worked material at 400°C, the irradiated and unirradiated material had similar ductilities, but the irradiated material had essentially no necking. The fracture surface was completely ductile in the case of unirradiated material but exhibited partial cleavage fracture in the case of irradiated material, consistent with the degradation of plastic deformation. Higher temperatures, however, resulted in failure entirely by ductile rupture. The case of 20%-cold-worked material was the most interesting in that the irradiated material had unexpectedly low ductilities at 525 and 700°C (Fig. 13). In both of these cases, the fracture mode was primarily ductile rupture, but some cleavage fracture was present (Fig. 17). This behavior was not repeated in the 30%-cold-worked material where complete ductile rupture was observed at 525 and 700°C. The prevalence of ductile rupture in the cold-worked material is evidence that the temperature of transition to ductile rupture is lowered by cold work.

Microstructural Observations

Transmission electron microscopy was performed on the specimens to aid in interpretation of the mechanical and fracture properties. Although no attempt was made to analyze swelling behavior or precipitation phenomena, general observations of these features will be discussed.

Helium-injected material — Helium-injected material was examined prior to testing, following testing, and following neutron irradiation.

No helium bubbles could be found despite a careful search of grain boundaries and matrix-precipitate interfaces.

Neutron-irradiated material exhibits a dense dislocation structure which coarsens with increasing temperature. This effect may be seen by comparing Fig. 18 where microstructures of specimens irradiated at 400 and 700°C are shown. Figure 18 also compares the specimen shoulder and gage sections; recall that helium was injected only into the gage sections. The microstructure appears nearly the same in the injected and noninjected regions, consistent with the similarity in strength. What appears to be a slightly coarser structure in Fig. 18(b) could have resulted from a higher temperature in the gage section during testing.

Cold-worked material — Figure 19 shows the structure of the 10, 20, and 30% cold worked material prior to irradiation. Consistent with the saturation in strength at the 10% cold work level, the dislocation density does not appear to vary significantly as cold work increases from 10 to 30%. The study of the effects of irradiation on the cold-worked material is really a study of the combination of cold work and recovery coupled with irradiation rather than a study of the effect of cold work alone. These effects are illustrated by the array of transmission electron micrographs shown in Fig. 20. The micrographs were selected to show representative dislocation structures in diffraction contrast for the three cold-work levels and three temperatures. Quantitative dislocation densities were not determined, but visual comparisons will be discussed. Two general trends in microstructural development are apparent in Fig. 20. As temperature increases, microstructure

coarsens. As cold work level increases, the microstructure coarsens. This is true at all three temperatures; defect density decreases moving up the figure. Both trends combine in the diagonal direction so that the micrograph in the lower left shows a much higher defect density than that in the upper right.

Swelling and Precipitation — No bubbles could be resolved in any material following helium injection. This is consistent with previous research on cyclotron implanted helium in vanadium and vanadium alloys where the implantation was below 200°C and not followed by annealing [9],[10],[11].

Voids were observed in both matrix material and precipitates. In all cases of matrix voids, swelling was below 0.001%. The largest matrix voids were 9 nm (Fig. 21), and no difference could be discerned between neutron-irradiated material that was injected with helium and that which was not helium injected. Voids were observed at all temperatures in annealed material, but in cold-worked material voids were observed only at 400°C at a cold-work level of 30%.

Precipitates were observed in all specimens including the starting material. Two precipitate morphologies were observed: blocky and larger rod-shaped precipitates. Similar rod-shaped precipitates were observed by Tanaka [9], and both blocky and rod precipitates were observed by Sprague et al. [10]. Although previously thought to be TiO_2 [9],[10], Braski has more recently analyzed precipitates using electron energy loss spectrometry and x-ray diffraction on extracted precipitates and identified titanium carbonitride [12]. Both precipitates may be present.

In the present study the blocky precipitates ranged in size from 50 to 1500 nm with the largest appearing at the highest irradiation temperature. The rod-like precipitates were generally larger ranging from 200 to 1500 nm as observed by Sprague et al., the largest appearing at the highest irradiation temperature [10]. Although a detailed study of precipitation was not made, the rod precipitates were observed only in irradiated material. No effect of helium injection was observed on the precipitates.

Cavities were frequently observed in both blocky and rod-like precipitates (Fig. 22). Cavities were observed in precipitates at all temperatures and cold-work levels. Precipitate cavities were usually comparable in size to matrix voids but exhibited a stronger temperature dependence. Cavities were found as large as 70 nm and were sometimes elongated in shape (Fig. 22) at 700°C.

DISCUSSION

Perhaps one of the most striking features of this study is the absence of helium embrittlement, intergranular fracture, and helium bubbles. The absence of helium bubbles in the matrix or on grain boundaries appears to be a result of the low implantation temperature. Tanaka also did not observe helium bubbles in V—20Ti implanted using the same method as that for V—15Cr—5Ti in the present study [9]. Implantation at higher temperature apparently allows the helium to diffuse sufficiently to form bubbles as observed by van Witzenburg et al. who implanted helium at 420 K [13]. The tritium trick method of doping which must be done at an elevated temperature results in numerous helium

bubbles in the matrix and at grain boundaries as observed by Braski [14]. The helium might have been expected to agglomerate into bubbles on grain boundaries during elevated temperature testing or during the two years of neutron irradiation. However, despite a careful search, no bubbles were found on grain boundaries in any specimens. Although this does not ensure that intergranular fracture resulting from helium will not occur, it is consistent with the observation that no specimens failed intergranularly. The absence of helium embrittlement in V—15Cr—5Ti is consistent with Santhanam et al. who observed helium embrittlement only at 750°C and above following cyclotron injection of 25 at. ppm He [2]. In V-Nb alloys and V—3Ti—1Si, Ehrlich and Böhn observed intergranular fracture only above 750°C [15]. However, Tanaka et al. found embrittlement resulting from intergranular fracture at 300°C in V—20Ti [9]. It appears that helium embrittlement resulting from cyclotron-implanted helium does not occur in V—15Cr—5Ti at 700°C and below. Nonetheless, since tritium trick doping results in embrittlement and since fusion reactor service has aspects of both helium introduction methods, caution should be used in interpretation of these results for fusion reactor application.

Despite the absence of what could be identified as helium embrittlement, there was clearly irradiation embrittlement. In all cases the low ductilities were accompanied by cleavage fracture. This might result from interstitial impurities or from radiation hardening. Since large amounts of precipitate were not found and since cold-worked specimens in the same irradiation vehicles were not embrittled, contamination by interstitial solutes is not considered most likely. The getter was

probably effective. However, the tangles of dislocation loops and segments observed by TEM are consistent with the observed matrix hardening, and the defect density is highest where cleavage fracture is most apparent.

The cleavage fracture observed at 400°C in annealed material becomes quasi-cleavage at 625°C and ductile rupture at 700°C. This is evidence that the cleavage stress was achieved prior to plastic flow until a temperature of about 625°C was reached, or the temperature of transition from brittle to ductile fracture occured at approximately 625°C.

The mechanism of radiation hardening is also evidenced by the embrittlement observed in the cold-worked material. Cold work appears to have the effect of retarding cleavage fracture. Perhaps the deformation and accompanying dislocations result in a higher energy for cleavage crack propagation since additional work is required to move dislocations during fracture, and surface energy is increased by cracking on multiple planes. However, a point is reached where the lattice hardening effect of dislocation tangles raises the yield stress above the cleavage stress and thus promotes cleavage fracture. It is possible that this mechanism is responsible for the abrupt decrease in elongation observed at 625 and 700°C at a cold-work level of 20%. When the cold-work level is increased still further, to 30%, the additional deformation energy promotes recovery. This was evident in Fig. 20 where it is shown that the dislocation density is lower in 30% cold-worked material than in 10 or 20% cold-worked material. This recovery resulted in sufficient softening to cause a return of ductile rupture

at the 30% cold-work level. Further investigation of this phenomenon is required since, at 700°C, there appears from the microstructure to be recovery at 20% cold work. The strength level is higher at the 20% level than at 10 and 30%, but experimental uncertainties do not permit conclusions to be drawn.

Although it is not within the scope of this paper to discuss swelling, it is clear that V—15Cr—5Ti is among the swelling resistant vanadium alloys. This observation agrees with that of Carlander et al. who observed no voids at 425°C at a fast fluence of 2×10^{26} n/m^2 [1] and Braski who observed less than 0.2% swelling at 40 dpa in helium doped material [14].

Tanaka observed minimal swelling in V—20Ti irradiated in the same vehicles as used in the present study [9]; Bentley and Wiffen did not find any voids in V—20Ti irradiated in EBR-II in the range 470—780°C at fluences in the range of 1.3 to 6.1×10^{26} n/m^2 (E > 0.1 MeV) [3].

The absence of helium bubbles is more difficult to explain since Tanaka observed them in V—20Ti [9]. Perhaps the presence of chromium results in a high degree of helium trapping, but clearly more work is needed to answer this question.

CONCLUSIONS

1. Cyclotron-injected helium at a level of 80 at. ppm has no significant effects on tensile, fracture, or microstructural properties of V—15Cr—5Ti between 400 and 700°C.

2. Ten percent cold work has a beneficial effect in reducing the tendency for cleavage fracture in irradiated V—15Cr—5Ti but higher

levels (certainly 20%) have a detrimental effect. Still higher levels are beneficial in that they induce recovery.

3. Tensile properties and microstructure indicate a high degree of recovery in 30% cold-worked material following irradiation at 700°C.

4. The temperature for transition from cleavage to ductile failure in neutron-irradiated (30 dpa) V—15Cr—5Ti is increased to approximately 625°C by irradiation hardening.

5. Swelling is negligible in V—15Cr—5Ti in the temperature range of 400—700°C at a fluence of 5×10^{26} n/m^2 ($E > 0.1$ MeV) (30 dpa).

6. Swelling was observed in precipitate particles which may be titanium carbonitrides or titanium oxides.

ACKNOWLEDGMENTS

The authors wish to thank D. N. Braski for many helpful discussions and assistance with electron microscopy. J. H. DeVan provided much useful information on liquid alkali metals. The authors also wish to thank D. N. Braski and R. L. Klueh for reviewing the manuscript. The assistance of B. L. Cox, C. K. Thomas, N. H. Rouse, L. T. Gibson, and E. L. Ryan with experimental work is most appreciated. J. W. Woods and A. F. Zulliger led the fabrication and design of the irradiation vehicle. The work of J. Young and F. A. Scarboro in typing the manuscript is also gratefully acknowledged.

REFERENCES

[1] R. Carlander, S. D. Harkness and A. T. Santhanam, Effect of Radiation on Structural and Mechanical Properties of Metals and Alloys, in: ASTM STP 529, American Society for Testing and Materials, 1973, p. 399.

[2] A. T. Santhanam, A. Taylor, and S. D. Harkness, Defects and defect clusters in bcc metals and their alloys, Nucl. Metal. 18 (1973) 302, Proc. Int. Conf. Gaithersburg, Md.

[3] J. Bentley and F. W. Wiffen, Nucl. Technol. 30 (1976) 376.

[4] T. A. Gabriel, B. L. Bishop, and F. W. Wiffen, Calculated Irradiation Response of Materials Using a Fusion-Reactor First-Wall Neutron Spectrum, ORNL/TM-5956 (Oak Ridge National Laboratory, June 1977) p. 5.

[5] J. F. Remark, A. B. Johnson, Jr., Harry Farrar IV, and D. G. Atteridge, Helium Charging of Metals by Tritium Decay, Nucl. Technol. 29 (1976) 369.

[6] R. L. Klueh, Miniature Tensile Test Specimens for Fusion Reactor Irradiation Studies, Nucl. Eng. & Design/Fusion 2 (1985) 407–416.

[7] H. E. Johnson, Chemistry, in Sodium-NaK Engineering Handbook, Vol. I, Gordon and Breach, 1972, pp. 253–254.

[8] J. R. Gibson and D. N. Braski, Scanning Electron Microscope Facility for Examination of Radioactive Materials, ORNL/TM-9451 (Oak Ridge National Laboratory, February 1985).

[9] M. P. Tanaka, E. E. Bloom, and J. A. Horak, Tensile Properties and Microstructure of Helium Injected and Reactor Irradiated V–20Ti, J. Nucl. Mater. 103&104 (1981) 895–900.

[10] J. A. Sprague, F. A. Smidt, Jr., and J. R. Reed, J. Nucl. Mater. 85&86 (1979) 739.

[11] F. A. Smidt and A. G. Pieper, Studies of the Mobility of Helium in Vanadium, J. Nucl. Mater. 51 (1974) 361–365.

[12] D. N. Braski, The Effect of Neutron Irradiation on Vanadium Alloys, Second Inter. Conf. on Fusion Reactor Materials, April 13–17, 1986, Chicago.

[13] W. van Witzenburg, A. Mastenbroek, and J. D. Elen, The Influence of Preimplanted Helium on the Microstructure of Neutron Irradiated Vanadium, J. Nucl. Mater. 103&104 (1981) 1187–1192.

[14] D. N. Braski, The Effect of Neutron Irradiation on the Tensile Properties and Microstructure of Several Vanadium Alloys, this conference.

[15] K. Ehrlich and H. Bohm, Proc. IAEA, Conference on Radiation Damage in Reactor Materials 2, p. 349, Vienna, Austria, 1969.

Table I. Composition of V—15Cr—5Ti
Heat HSV-307

Element	(wt %)	Element	(wt %)
Cr	14.8	Ni	0.004
Cu	0.02	P	0.0003
Fe	0.07	S	<0.001
Mn	0.001	Ti	4.8
Mo	0.03	Zr	0.01
Nb	0.02	V	bal

Table II. Tensile properties

Specimen	Condition	Test temperature (°C)	Strength (MPa)		Elongation (%)	
			Yield	Ultimate tensile	Uniform	Total
		Controls				
100C	Annealed	400	491	610	7.4	8.9
104C	Annealed	525	422	574	8.0	10.0
106C	Annealed	525	423	586	8.3	9.8
101C	Annealed	625	417	621	8.9	10.3
103C	Annealed	625	405	621	9.3	11.1
102C	Annealed	700	403	574	9.2	15.2
3C	10% CW	400	672	769	1.1	2.6
15C	10% CW	525	655	774	0.86	1.9
14C	10% CW	700	517	683	2.4	6.9
4C	20% CW	400	724	827	1.1	2.1
13C	20% CW	525	603	796	1.0	1.8
2C	20% CW	700	543	707	2.1	5.6
14C	20% CW	700	517	698	2.3	5.3
2C	30% CW	400	724	827	1.1	2.7
8C	30% CW	525	603	814	1.1	2.3
6C	30% CW	700	483	698	2.3	6.1
		Helium Implanted				
3-64	Annealed	400	503	574	4.4	5.9
1-8	Annealed	400	512	590	2.1	3.5
1-55	Annealed	525	479	582	7.0	9.2
1-68	Annealed	625	396	581	9.2	11.2
3-57	Annealed	700	336	531	10.0	12.3
1-58	Annealed	700	365	548	12.1	15.3
		Neutron Irradiated				
7	Annealed	625	776	853	0.38	0.50
8	Annealed	700	738	943	0.94	0.94
9	10% CW	400	1140	1260	1.1	1.2
6	10% CW	525	819	972	4.2	4.9
16	10% CW	700	608	883	1.9	6.6
11	20% CW	400	1130	1220	1.3	1.4
12	20% CW	400	1100	1200	0.94	1.0
7	20% CW	525	710	853	1.0	1.0
19	20% CW	700	612	1000	1.8	1.8
15	30% CW	400	1130	1210	0.92	1.2
11	30% CW	525	664	910	3.3	3.6
17	30% CW	700	434	533	2.3	4.4
		Helium Implanted Plus Neutron Irradiated				
1-80	Annealed	400	991	1170	0.76	0.76
1-72	Annealed	700	741	822	2.0	3.0

Table III. Fracture surface morphology

	400°C	525°C	625°C	700°C
		Annealed		
Unirradiated	Ductile		Ductile	Ductile
Helium implanted	Ductile			Ductile
Neutron irradiated			Quasi-cleavage	Ductile
Helium implanted plus neutron irradiated	Cleavage			Ductile
		10%-cold work		
Unirradiated	Ductile	Ductile		Ductile
Neutron irradiated	Ductile/ cleavage	Ductile		Ductile
		20%-cold work		
Unirradiated	Ductile	Ductile		Ductile
Neutron irradiated	Quasi-cleavage/ cleavage	Ductile/ cleavage		Ductile/ cleavage
		30%-cold work		
Unirradiated	Ductile	Ductile		Ductile
Neutron irradiated	Ductile/ cleavage	Ductile		Ductile

List of Figures

Fig. 1. Sheet tensile specimen.

Fig. 2. Tensile and 0.2% yield stress as a function of test temperature for annealed V—15Cr—5Ti.

Fig. 3. Uniform and total elongation as a function of test temperature for annealed V—15Cr—5Ti.

Fig. 4. Tensile and 0.2% yield stress as a function of test temperature for 10% cold-worked V—15Cr—5Ti.

Fig. 5. Tensile and 0.2% yield stress as a function of test temperature for 20% cold-worked V—15Cr—5Ti.

Fig. 6. Tensile and 0.2% yield stress as a function of test temperature for 30% cold-worked V—15Cr—5Ti.

Fig. 7. Uniform and total elongation as a function of test temperature for 10% cold-worked V—15Cr—5Ti.

Fig. 8. Uniform and total elongation as a function of test temperature for 20% cold-worked V—15Cr—5Ti.

Fig. 9. Uniform and total elongation as a function of test temperature for 30% cold-worked V—15Cr—5Ti.

Fig. 10. Yield strength as a function of cold-work level (reduction of area) for unirradiated V—15Cr—5Ti.

Fig. 11. Yield strength as a function of cold-work level (reduction of area) for V—15Cr—5Ti irradiated in EBR-II to 28 to 32 dpa.

Fig. 12. Total tensile elongation as a function of cold-work level (reduction of area) for unirradiated V—15Cr—5Ti.

Fig. 13. Total tensile elongation as a function of cold-work level (reduction of area) for V—15Cr—5Ti irradiated in EBR-II to 28 to 32 dpa.

Fig. 14. Fracture surface of unirradiated 10% cold-worked V—15Cr—5Ti specimen No. 3c fractured at 400°C.

Fig. 15. Fracture surface of annealed V—15Cr—5Ti irradiated at 625°C and fractured at room temperature.

Fig. 16. Fracture surfaces of annealed V—15Cr—5Ti irradiated to 30 dpa showing range of surface morphologies. (a) Specimen No. 1-80 containing 80 appm He irradiated and tested at 400°C; (b) specimen No. 7 irradiated and tested at 625°C; (c) specimen No. 8 irradiated and tested at 700°C.

Fig. 17. Portion of the fracture surface showing cleavage in 20% cold-worked V—15Cr—5Ti irradiated to 30 dpa at 700°C and tensile tested at 700°C.

Fig. 18. Microstructure of V—15Cr—5Ti irradiated to 30 dpa. (a) Shoulder of specimen No. 1-80 containing no helium; (b) gage section of specimen No. 1-80 containing 80 appm He; (c) specimen No. 8 irradiated and tested at 700°C.

Fig. 19. Microstructure of unirradiated 10, 20, and 30% cold-worked V—15Cr—5Ti.

Fig. 20. Microstructure of cold-worked V—15Cr—5Ti following irradiation to 30 dpa. No helium has been injected into these specimens. The effects of cold work and recovery may be seen.

Fig. 21. Matrix voids in 30%-cold-worked V—15Cr—5Ti (specimen No. 15) irradiated to 30 dpa at 400°C.

Fig. 22. Voids in blocky precipitate in 10% cold-worked V—15Cr—5Ti (specimen No. 16) irradiated to 30 dpa at 700°C.

ORNL-DWG 78-7703R

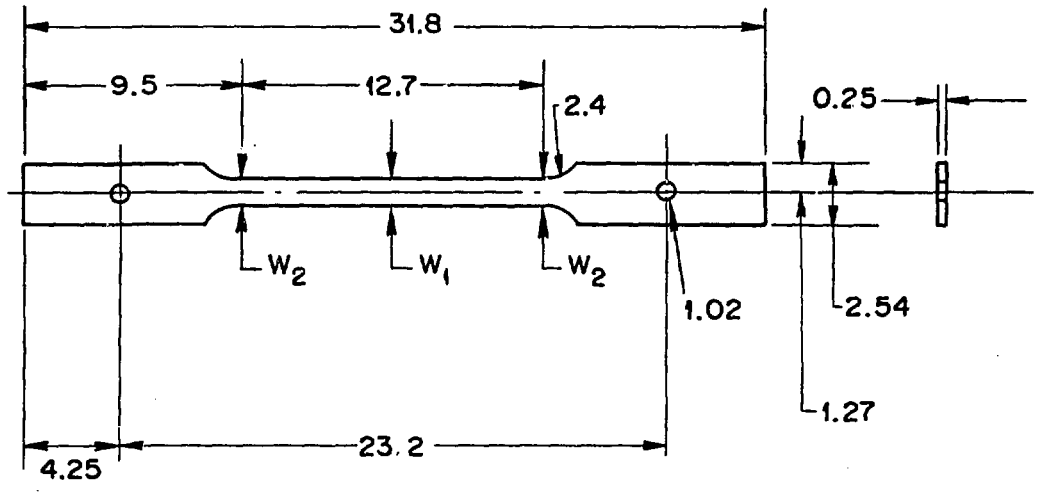

W_1 = 1.02 WIDTH

W_2 = FROM 0.005 TO 0.013 GREATER THAN W_1

DIMENSIONS IN MILLIMETERS

Fig. 1. Sheet tensile specimen.

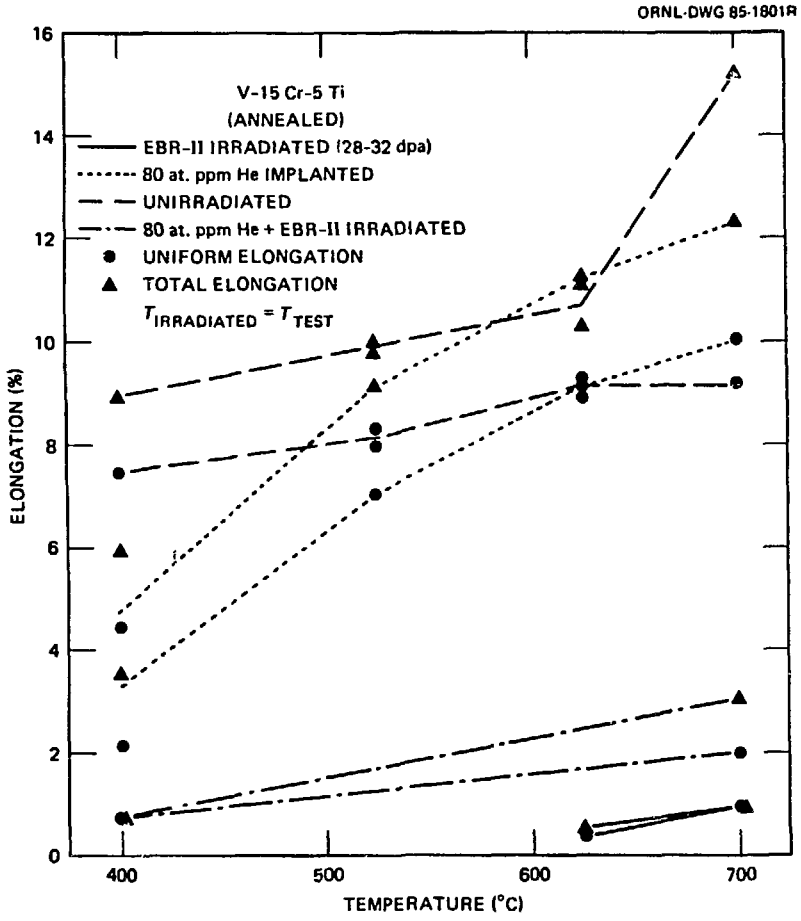

Fig. 3. Uniform and total elongation as a function of test temperature for annealed V–15Cr–5Ti.

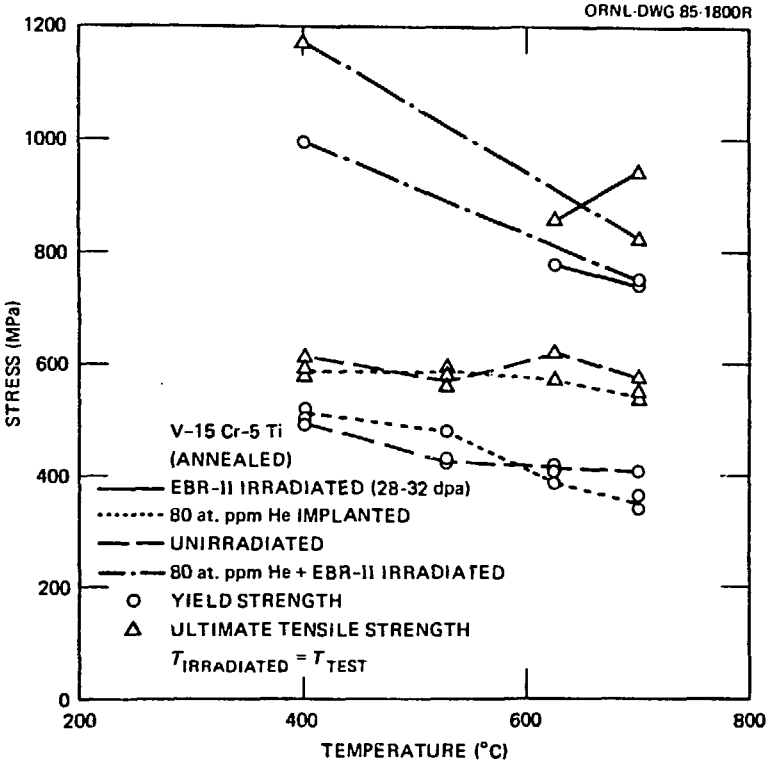

Fig. 2. Tensile and 0.2% yield stress as a function of test temperature for annealed V–15Cr–5Ti.

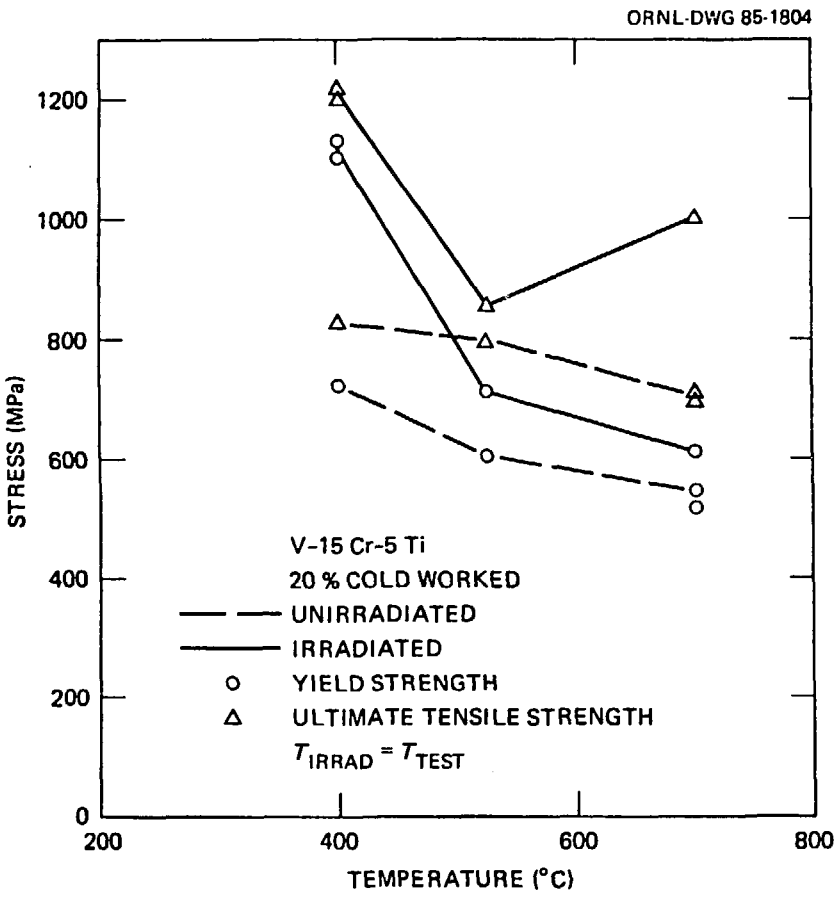

Fig. 5. Tensile and 0.2% yield stress as a function of test temperature for 20% cold-worked V—15Cr—5Ti.

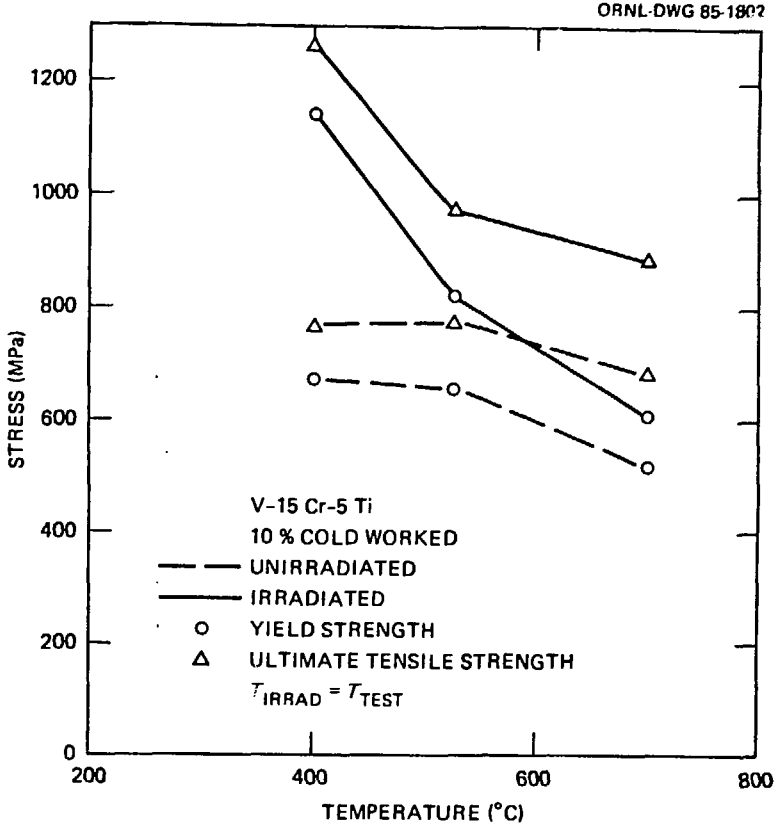

Fig. 4. Tensile and 0.2% yield stress as a function of test temperature for 10% cold-worked V—15Cr—5Ti.

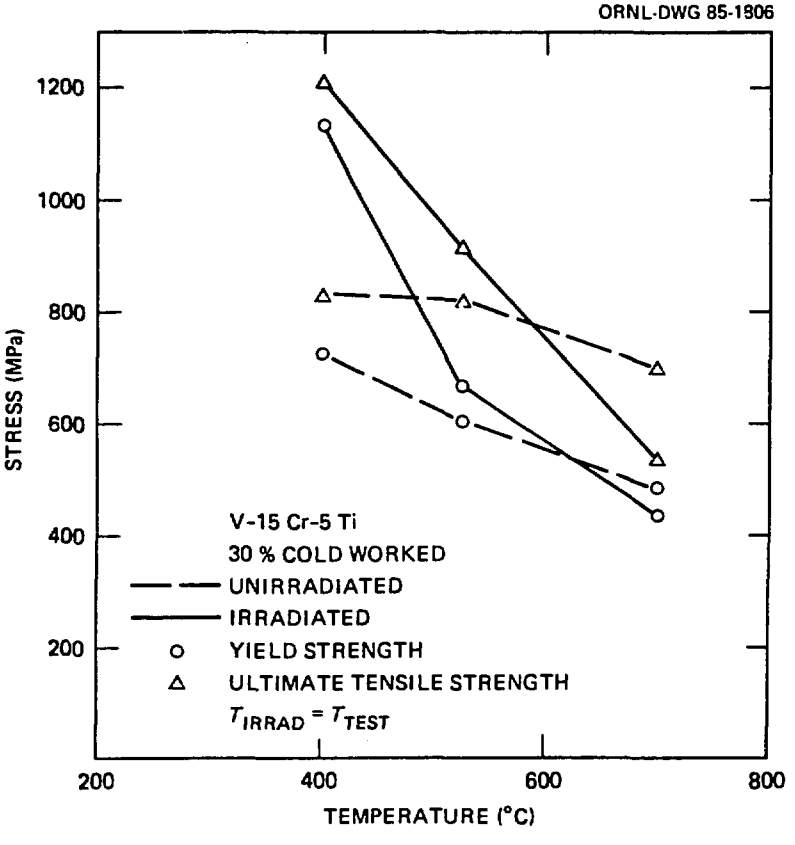

Fig. 6. Tensile and 0.2% yield stress as a function of test temperature for 30% cold-worked V—15Cr—5Ti.

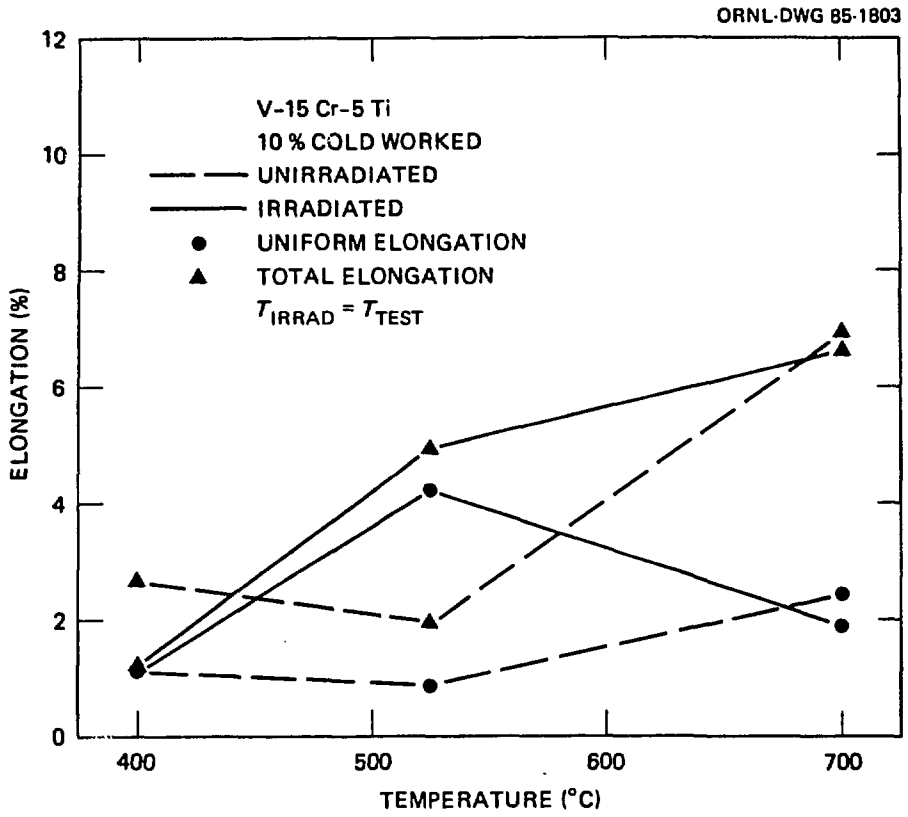

Fig. 7. Uniform and total elongation as a function of test temperature for 10% cold-worked V—15Cr—5Ti.

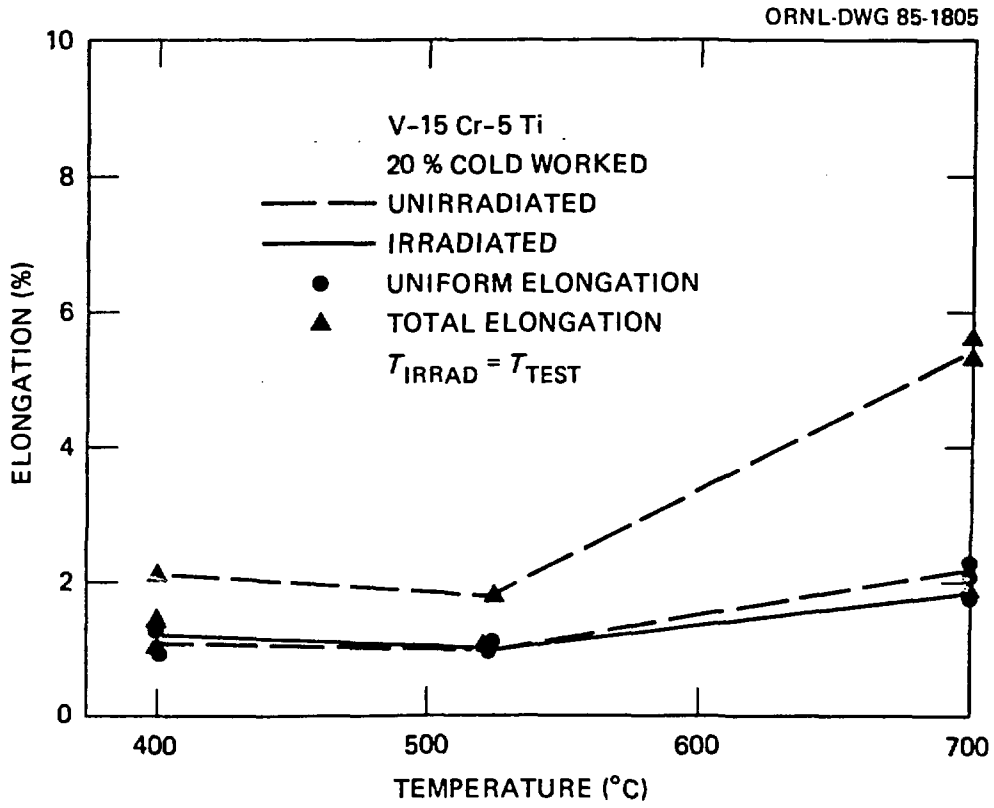

Fig. 8. Uniform and total elongation as a function of test temperature for 20% cold-worked V—15Cr—5Ti.

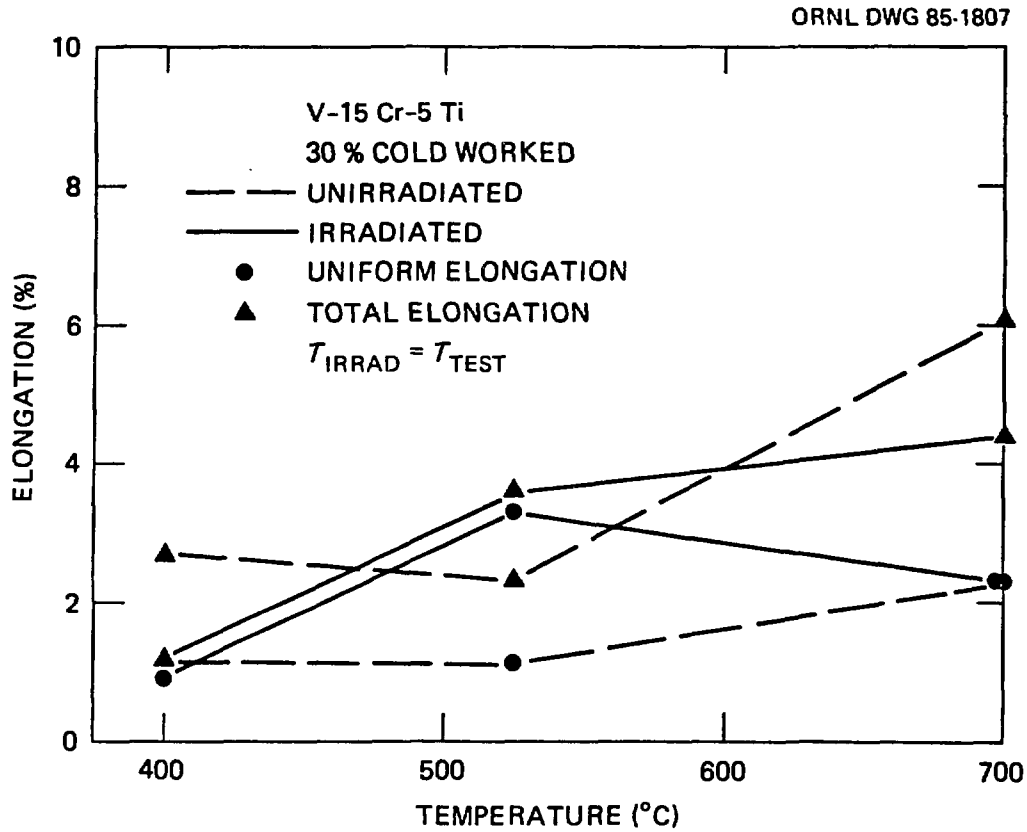

Fig. 9. Uniform and total elongation as a function of test temperature for 30% cold-worked V—15Cr—5Ti.

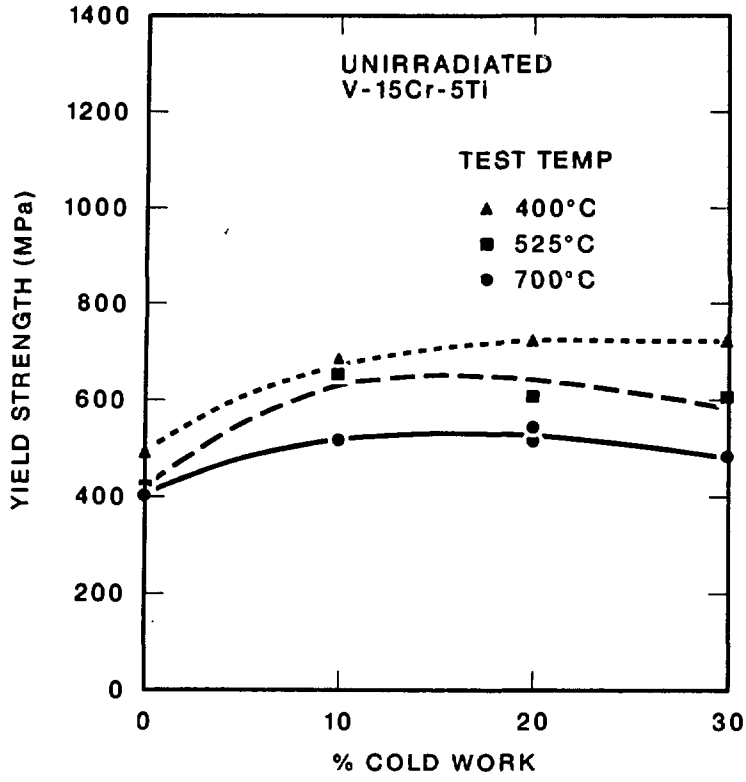

Fig. 10. Yield strength as a function of cold-work level (reduction of area) for unirradiated V—15Cr—5Ti.

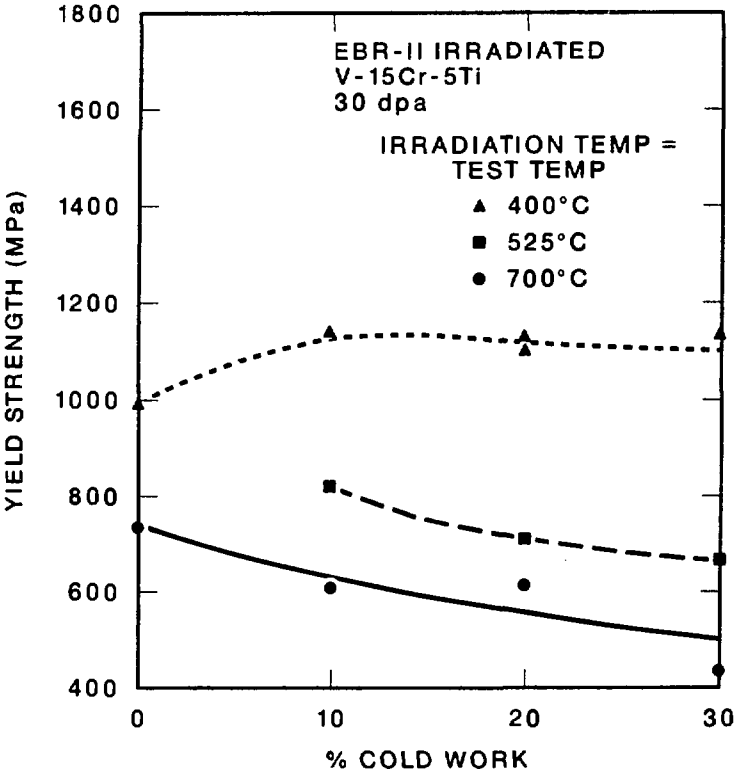

Fig. 11. Yield strength as a function of cold-work level (reduction of area) for V—15Cr—5Ti irradiated in EBR-II

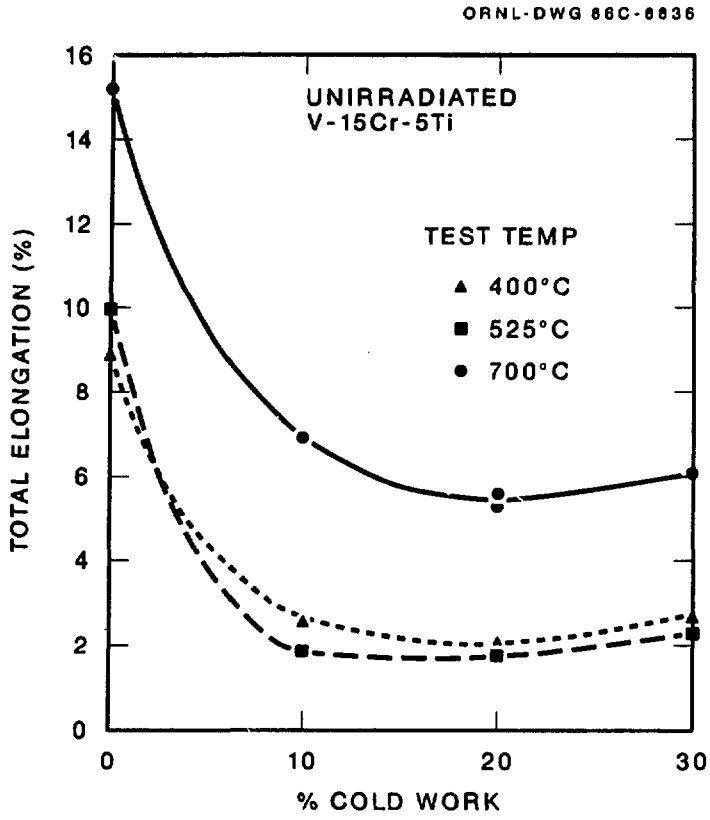

Fig. 12. Total tensile elongation as a function of cold-work level (reduction of area) for unirradiated V—15Cr—5Ti.

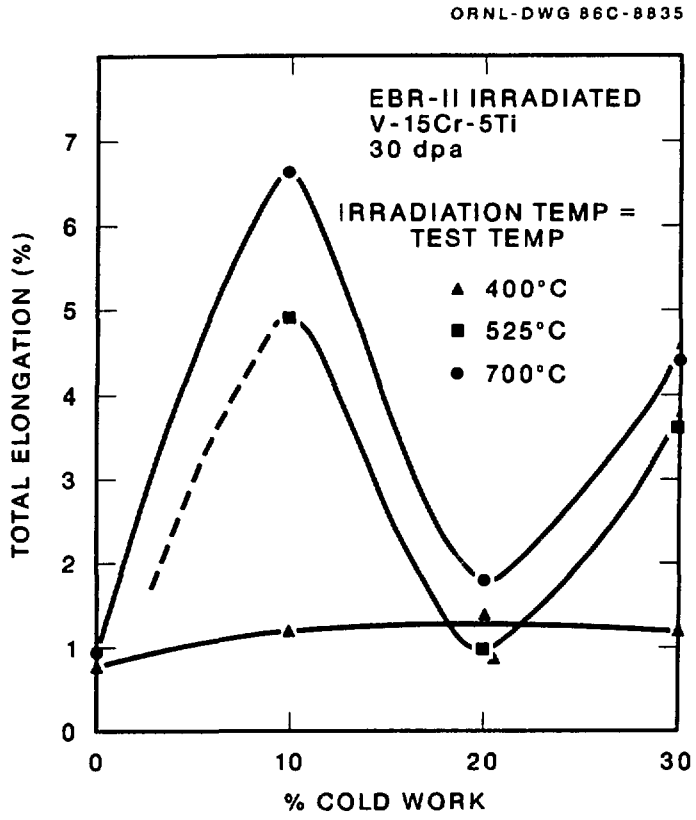

Fig. 13. Total tensile elongation as a function of cold-work level (reduction of area) for V—15Cr—5Ti irradiated in EBR-II to 30 dpa at 400, 525, and 700°C.

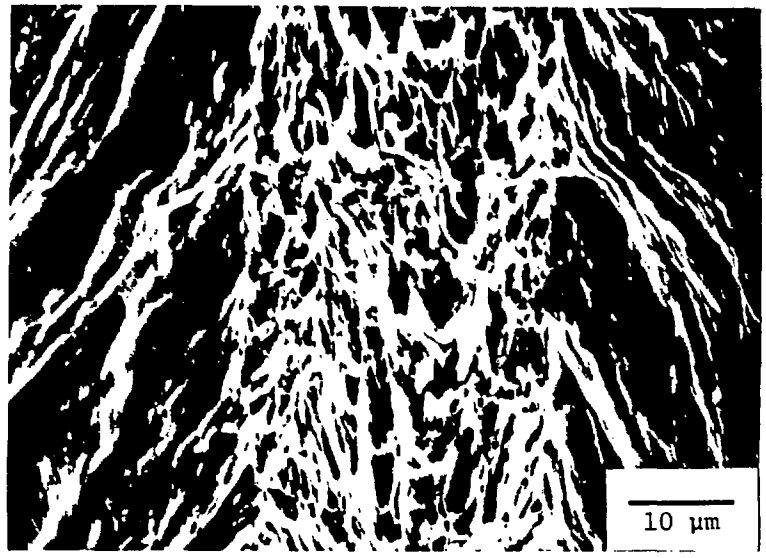

Fig. 14. Fracture surface of unirradiated 10% cold-worked V—15Cr—5Ti specimen No. 3c fractured at 400°C.

Fig. 15. Fracture surface of annealed V—15Cr—5Ti irradiated at 625°C and fractured at room temperature.

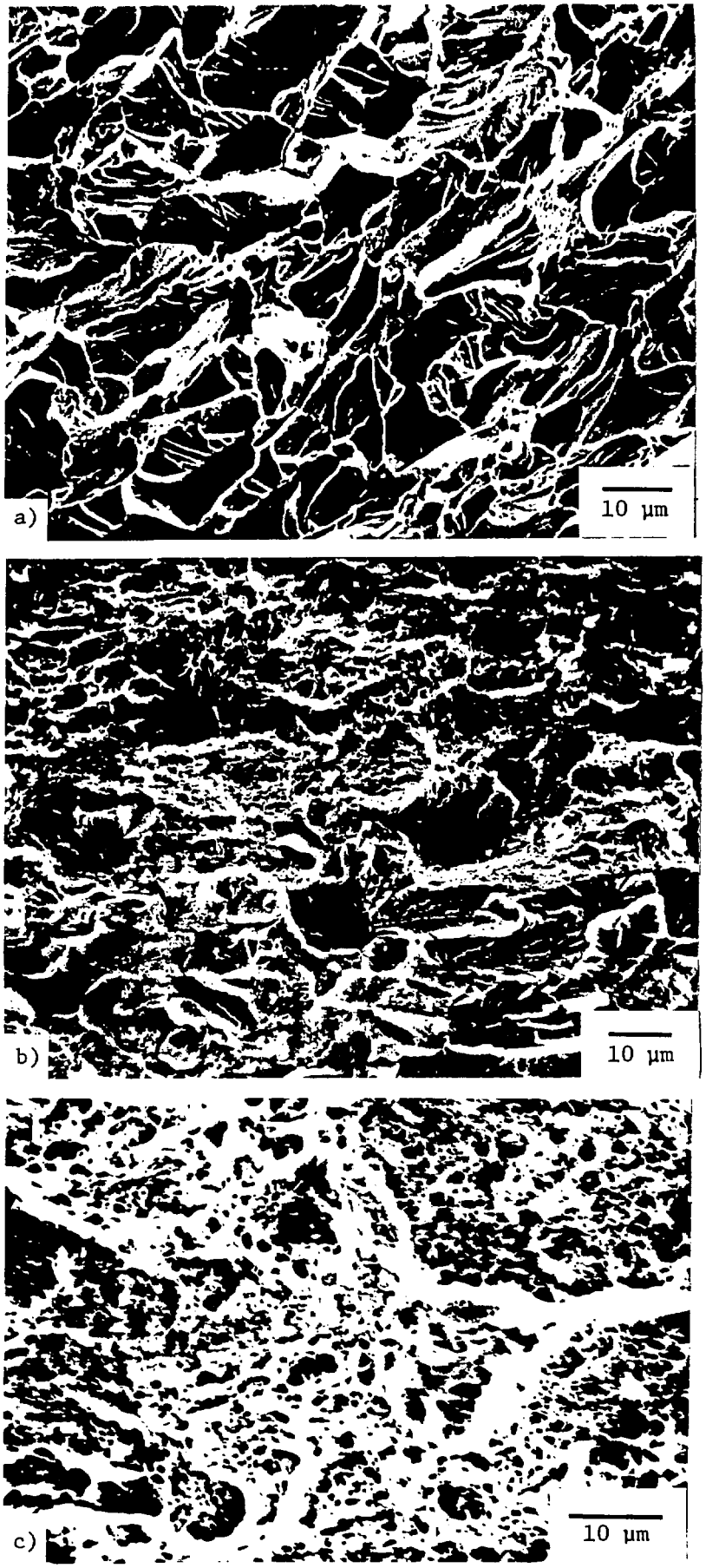

Fig. 16. Fracture surfaces of annealed V–15Cr–5Ti irradiated to 30 dpa showing range of surface morphologies. (a) Specimen No. 1-80 containing 80 appm He irradiated and tested at 400°C; (b) specimen No. 7 irradiated and tested at 625°C; (c) specimen No. 8 irradiated and

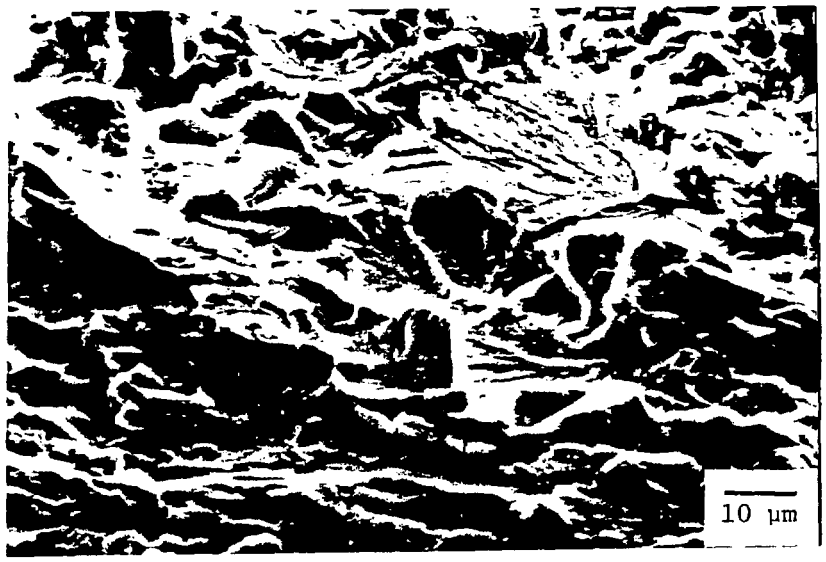

Fig. 17. Portion of the fracture surface showing cleavage in 20% cold-worked V—15Cr—5Ti irradiated to 30 dpa at 700°C and tensile tested at 700°C.

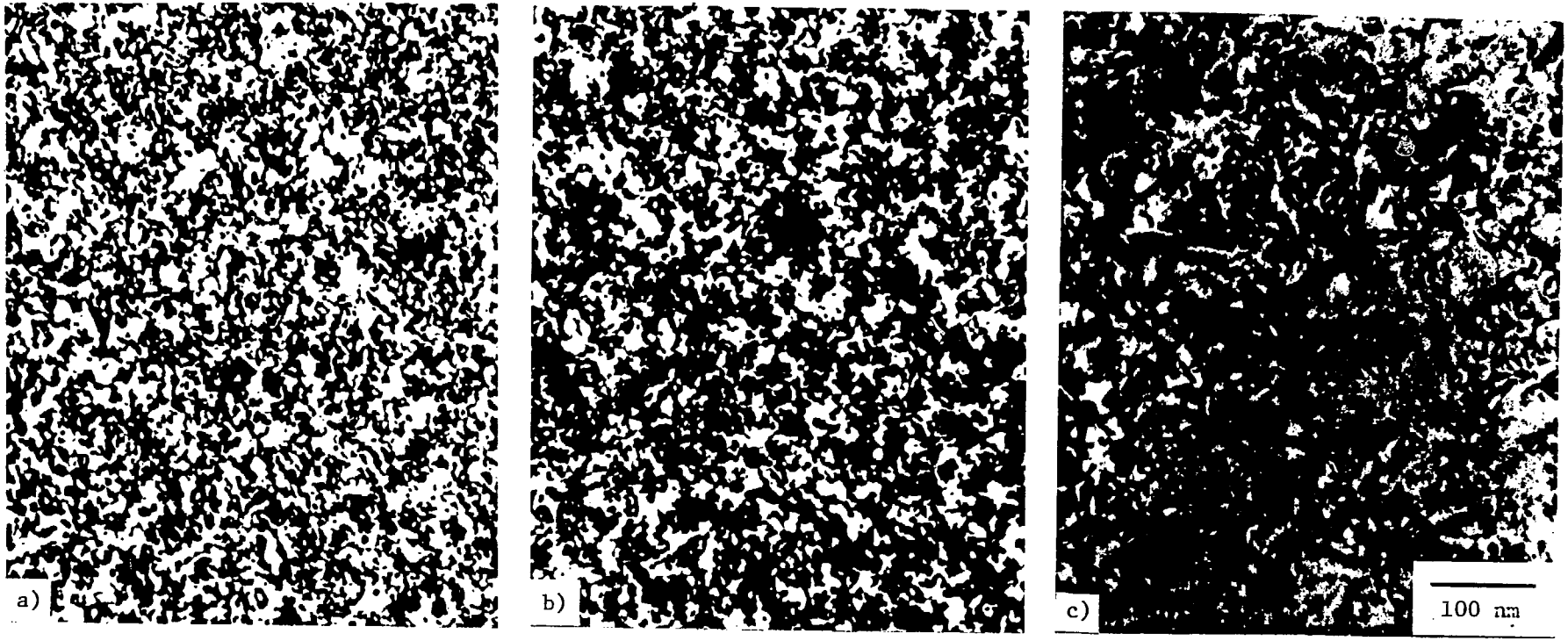

Fig. 18. Microstructure of V—15Cr—5Ti irradiated to 30 dpa. (a) Shoulder of specimen No. 1-80 containing no helium; (b) gage section of specimen No. 1-80 containing 80 appm He; (c) specimen No. 8 irradiated and tested at 700°C.

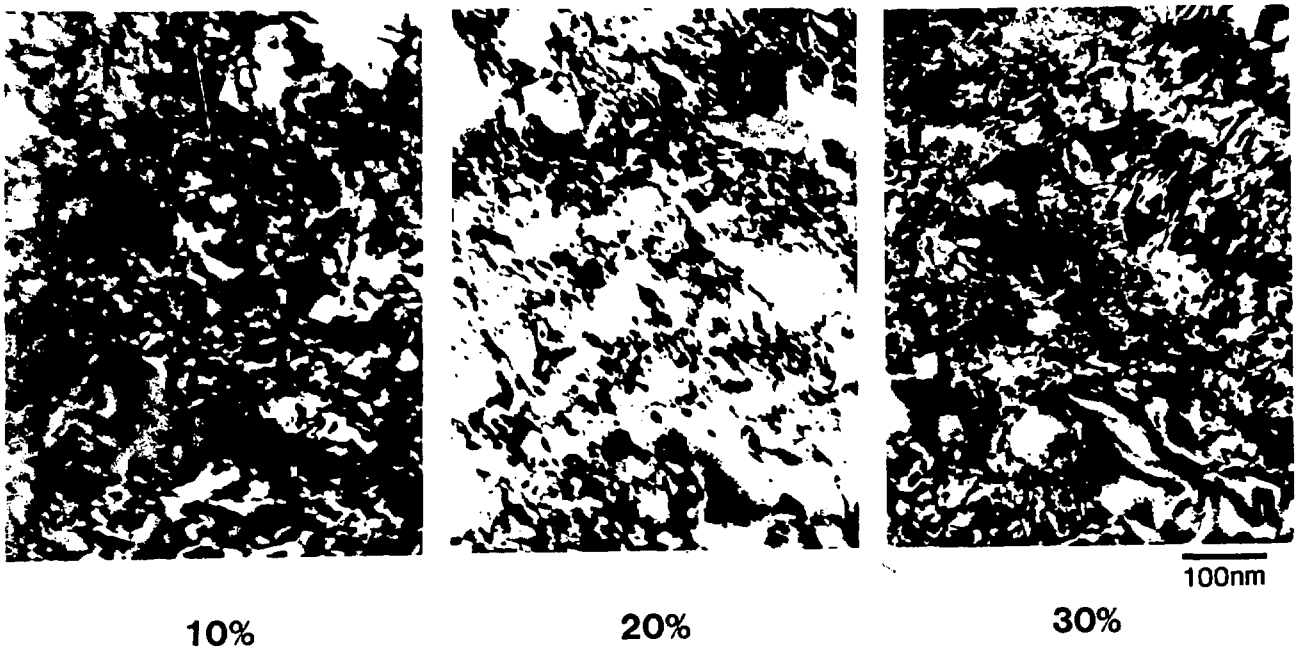

Fig. 19. Microstructure of unirradiated 10, 20, and 30% cold-worked V—15Cr—5Ti.

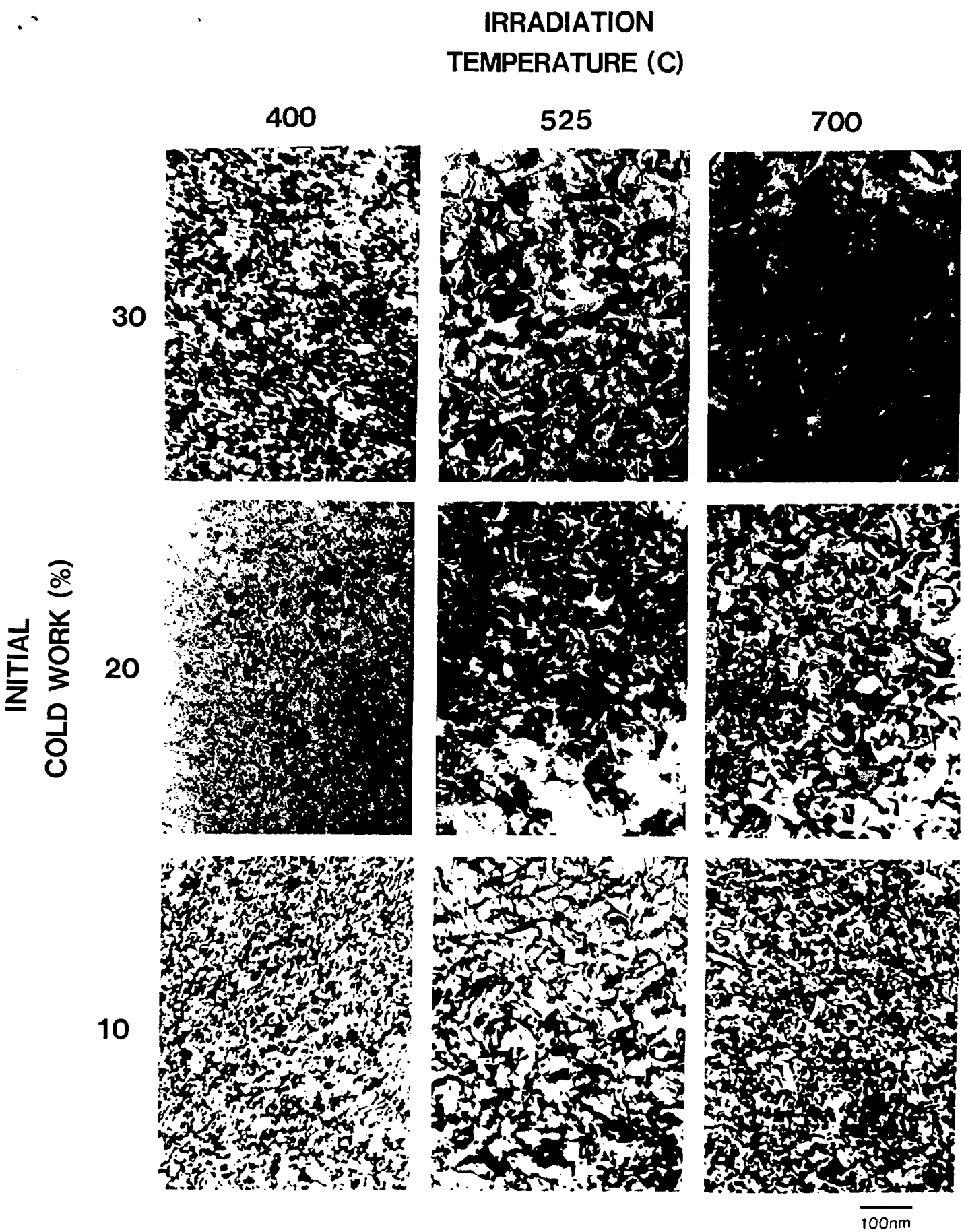

Fig. 20. Microstructure of cold-worked V—15Cr—5Ti following irradiation to 30 dpa. No helium has been injected into these specimens. The effects of cold work and recovery may be seen.

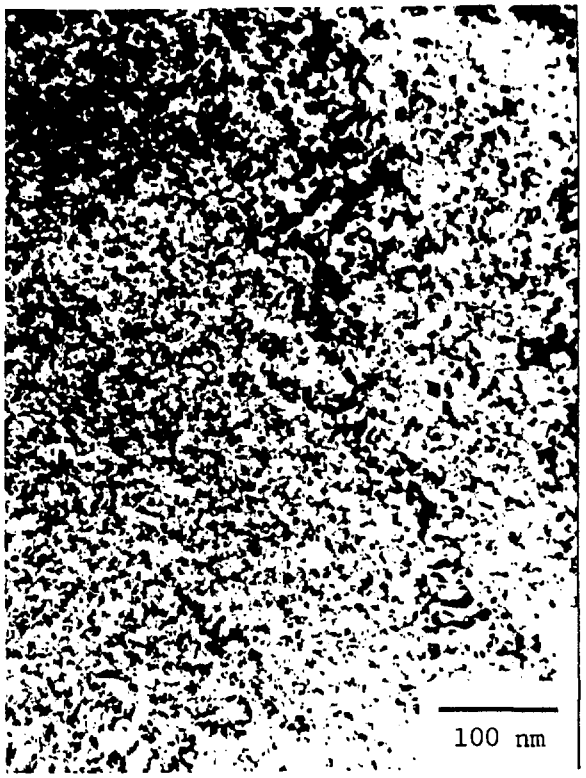

Fig. 21. Matrix voids in 30%-cold-worked V—15Cr—5Ti (specimen No. 15) irradiated to 30 dpa at 400°C.

Fig. 22. Voids in blocky precipitate in 10% cold-worked V—15Cr—5Ti (specimen No. 16) irradiated to 30 dpa at 700°C.